Surface Characterization of Tyrosine-Derived Polycarbonates

VÍCTOR H. PÉREZ-LUNA,[1] KIMBERLY A. HOOPER,[2] JOACHIM KOHN,[2] BUDDY D. RATNER[1,3]

[1] Department of Chemical Engineering, Box 351750, University of Washington, Seattle, Washington 98195

[2] Department of Chemistry, Rutgers, The State University of New Jersey, New Brunswick, New Jersey 08903

[3] Center for Bioengineering, Box 351750, University of Washington, Seattle, Washington 98195

ABSTRACT: The surfaces of five biodegradable tyrosine-derived polycarbonates were studied using contact angle measurements, ESCA, and static SIMS. The wettability, critical surface tension, and polarity of these polymers decreased with increasing chain length of the pendent alkyl groups. Surface elemental composition, as determined by ESCA, was consistent with the stoichiometry of the repeat unit of the polymers. High-resolution C1s, O1s, and N1s ESCA spectra also showed results consistent with the different bonding states of these elements in the polymer repeat unit. In both positive and negative ion spectra, SIMS experiments showed fragment ions characteristic of the polymer backbone. Fragment ions characteristic of the pendent groups were identified in the negative ion SIMS spectra only, while the positive SIMS spectra provided a characteristic fingerprint for each polymer. © 1997 John Wiley & Sons, Inc. J Appl Polym Sci **63:** 1467–1479, 1997

Key words: surface analysis; ESCA; SIMS; tyrosine; polycarbonates; biomaterials; contact angle

INTRODUCTION

Biodegradable polymers are used in temporary medical implants such as resorbable sutures,[1] small bone fixation devices,[2] and drug-delivery systems.[3] Biodegradable polymers for the design of temporary scaffolds for tissue regeneration represents an additional application that is currently under intense investigation.[4,5] These applications impose stringent requirements on the physical, chemical, and mechanical properties of the polymers while biocompatibility concerns and the potential toxicity of the polymer and its degradation

products limit the choice of acceptable monomers used in polymer design and synthesis.

A fundamental principle in biomaterials research is that the surface properties of a synthetic material influence the biological response.[6,7] When an implant is placed in contact with a biological system, proteins and cells interact directly with the material surface. Thus, the state of the surface is a determining factor in the blood compatibility and/or tissue response elicited by the implant.[6] Because of the importance of the surface in biological interactions with synthetic materials, characterization of the surface is essential. In general, no single technique can give a complete picture of the surface. Therefore, it is necessary to use a number of surface analysis techniques that provide complementary information in order to gain insight into the surface properties of synthetic materials.

Using contact angle measurements, electron spectroscopy for chemical analysis (ESCA) and static secondary ion mass spectrometry (SIMS), we report here the surface characterization and the surface properties of five tyrosine-derived polycarbonates. These materials represent a specific example of pseudo-poly(amino acids), a new class of polymers in which derivatives of naturally occurring amino acids are linked together into a polymeric chain by nonamide bonds.[8-10] While most conventional poly(amino acids) are insoluble, nonmelting materials that are expensive to prepare and difficult to process,[11] the presence of nonamide bonds in the polymeric backbone greatly improves the physicomechanical properties and processability of pseudo-poly-(amino acids).[9] At the same time, the use of naturally occurring amino acids as the polymeric building blocks can reduce the potential toxicity of degradation products released into the biological system.

In the synthesis of tyrosine-derived polycarbonates, L-tyrosine (Tyr) and its natural metabolite desaminotyrosine [3-(4′-hydroxphenyl)propionic acid] (Dat) were used as building blocks to form desaminotyrosyl–tyrosine alkyl esters (Fig. 1). These diphenolic monomers were then polymerized to provide tyrosine-derived polyiminocarbonates,[12] polycarbonates,[13,14] and polyarylates.[15] The versatility of desaminotyrosyl–tyrosine alkyl esters as monomers resides not only in the capability of introducing different types of linkages into the polymeric backbone, but also in the possibility of modifying the properties of these materials by introducing different pendent groups.[12,13] The pendent groups of the polycarbonates reported in this article consist of ethyl, butyl, hexyl, octyl, and benzyl esters. The corresponding polymers are referred to as poly(DTE carbonate), poly(DTB carbonate), poly(DTH carbonate), poly(DTO carbonate), and poly(DTBzl carbonate) respectively (Fig. 1).

These tyrosine-derived polycarbonates have been studied before and have shown good biocompatibility *in vitro*[14] and *in vivo*.[16-18] The work presented here complements the previously reported biocompatibility studies[14,16,17] and provides a point of reference for the surface characterization of these materials and their analogs such as polyiminocarbonates[12] and polyarylates.[15]

EXPERIMENT

Polymer Synthesis

Poly(DTE carbonate), poly(DTB carbonate), poly(DTH carbonate), and poly(DTO carbonate)
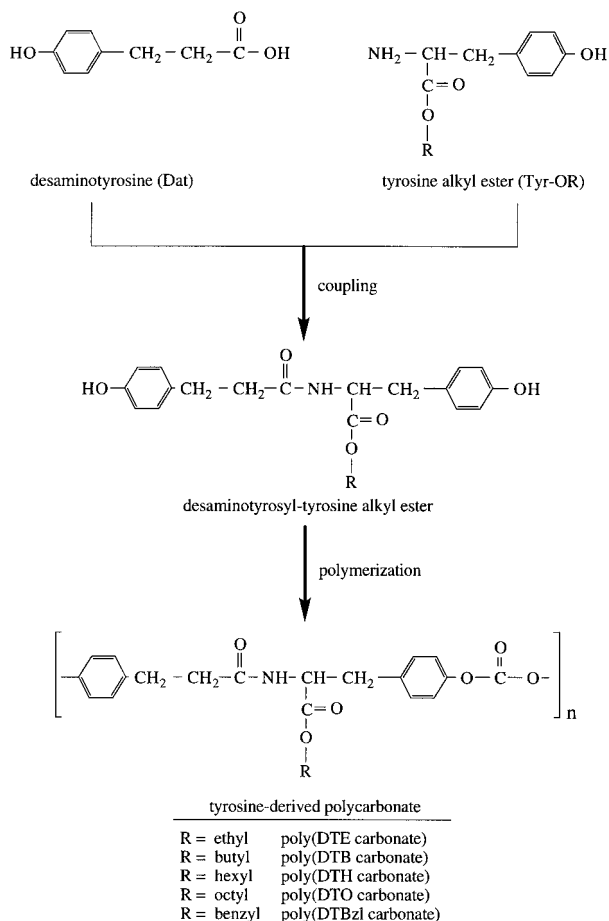

Figure 1 Synthetic scheme and chemical structure of desaminotyrosyl–tyrosine alkyl esters and the resulting polycarbonates.

were synthesized according to published procedures.[13,14,19] Poly(DTBzl carbonate) was synthesized using the methods described by Ertel and Kohn[14] with the following modifications. The *p*-toluenesulfonate salt of tyrosine benzyl ester was obtained from Sigma (St. Louis, MO). Following coupling with dicyclohexyl carbodiimide and 1-hydroxybenzotriazole hydrate, the crude reaction mixture was purified by column chromatography using ethyl acetate : hexane (6 : 4) as the mobile phase.

Polymer Characterization

Fourier transform infrared spectroscopy (FTIR) (performed on a Magnus Cygnus 100 spectrometer) and [1]H-nuclear magnetic resonance (NMR) (performed on a Varian Gemini 200) were used to confirm the polymer structure. Molecular weights of polymers were measured on a gel per-

meation chromatography (GPC) chromatographic system consisting of a Perkin-Elmer Model 410 pump, a Waters Model 410 refractive index detector, and a Perkin-Elmer Model 2600 computerized data station. Two PL-gel GPC columns (10^5 and 10^3 Å pore size, 30 cm length) were operated in series at a flow rate of 1 mL/min in methylene chloride. Molecular weights were calculated relative to polystyrene standards (Polymer Laboratories, Ltd., Church Stretton, UK) without further corrections.

Sample Preparation

Prior to spin casting, the polymers were dissolved in methylene chloride (2% w/v) and filtered through 0.5 μm Teflon filters from Millipore (#SLGS025OS). Glass disks (12 mm diameter) obtained from TED PELLA, Inc., (Redding, CA) were cleaned by sonication in a 4% Isopanasol solution (C. R. Callen Corp., Seattle, WA); this was followed by extensive rinsing and sonication in distilled water. Then, polymer films were centrifugally cast onto the glass disks. Typically, 20–25 μL of the polymer solution was pipetted onto a glass disk spinning at 4000 rpm for 20 s on an EC-01 spin coater (Headway Research Inc., Garland, TX) in a laminar flow hood.

Surface Analysis

Contact angles were measured using a Ramé-Hart Model 100-00-00NRL goniometer (Ramé-Hart, Inc., Mountain Lakes, NJ) as described previously.[20] A minimum of 18 measurements of advancing contact angles were made for each liquid (water, glycerol, formamide, thiodiglycol, and methylene iodide) on each of the polymeric surfaces. From the data, the critical surface tension (γ_c) of the polymers was obtained using Zisman's method;[21] the dispersive component of surface tension (γ^d) and the polar component of surface tension (γ^p) were calculated using the geometric mean approximation to the work of adhesion for dispersive and polar interactions as proposed by Kaelble et al.[22,23]

The parameters γ^d and γ^p were determined by minimizing the error in the fitting eq. (1), using the Nelder–Mead simplex algorithm, i.e., the criteria used to fit the data to eq. (1) were such that the parameters obtained (γ^d and γ^p) predicted the best fit to the observed data, θ, rather than $\cos \theta$:

$$\theta = \cos^{-1}\left(\frac{2\sqrt{\gamma_1^d \gamma_s^d} + 2\sqrt{\gamma_1^p \gamma_s^p}}{\gamma_1} - 1\right) \quad (1)$$

Surfaces were analyzed by ESCA using a Surface Science Instruments Model SSX-100 spectrometer at the National ESCA and Surface Analysis Center for Biomedical Applications, University of Washington. This system permitted the analysis of the outermost 50 Å of a sample in an elliptical area whose short axis was adjusted to 1000 μm. An AlK$\alpha_{1,2}$ monochromatized X-ray source ($h\nu = 1486.6$ eV) was used to stimulate photoemission. An electron flood gun set at 5 eV was used to minimize surface charging of the samples during the acquisition of ESCA spectra. The energy of the emitted electrons was measured with a hemispherical analyzer. Survey scans from 0 to 1000 eV binding energy (with a pass energy of 150 eV) were performed to determine the elemental composition of the surfaces. At this pass energy, the transmission function of the spectrometer can be assumed to be constant (information provided by the instrument manufacturer). The peak areas were normalized by the number of scans, points per eV, Scofield photoemission cross sections,[24] and sampling depth. The sampling depth can be assumed to vary as $KE^{0.7}$, where KE is the kinetic energy of the photoelectrons (information provided by the instrument manufacturer). All ESCA data was acquired at a photoelectron take-off angle of 55°; the take-off angle was defined as the angle between the surface normal and the axis of the analyzer lens. High-resolution scans of the carbon 1s (C1s), oxygen 1s (O1s), and nitrogen 1s (N1s) region (50 eV pass energy window) were also recorded and the $\underline{CH}_x$ peaks were assigned to 285.0 eV.[25] The spectral envelopes were resolved into several Gaussian peaks using SSI data analysis software to peak fit the spectra.

Static SIMS analysis were performed on a Model 7200 time of flight (TOF)–SIMS instrument from Physical Electronics (PHI) (Eden Prairie, MN) equipped with a 8 keV Cs$^+$ ion source and a two-stage reflectron time-of-flight mass analyzer. The total accumulated ion dose per sample was kept below 10^{13} ions/cm^2 to ensure that static SIMS conditions were met.[26]

RESULTS AND DISCUSSION

Polymer Synthesis

The weight-average molecular weight of the polycarbonates used ranged from 100,000 to 300,000

Table I   Molecular Weights of Tyrosine-derived Polycarbonates Used in This Study

Polymer	Weight Average (M_w)	Number Average (M_n)	Polydispersity (M_w/M_n)
Poly(DTE carbonate)	100,000	47,000	2.12
Poly(DTB carbonate)	123,000	53,000	2.16
Poly(DTH carbonate)	177,000	80,000	2.21
Poly(DTO carbonate)	300,000	115,000	2.60
Poly(DTBzl carbonate)	237,000	94,000	2.52

Daltons (Table I). All polymers were purified by dissolution in methylene chloride and precipitation in methanol or isopropanol to remove low molecular weight species. The polymers were redissolved in methylene chloride and precipitated into hexane at least one time to remove any silicon contamination. The structure of each polymer was verified by NMR and FTIR.

Contact Angle Measurements

The contact angle measurements for each of the tyrosine-derived polycarbonates was obtained for five different liquids (Table II). The wettability of these polymers decreased with increasing length of the pendent alkyl chain for the homologous series of ethyl to octyl. There are two explanations for the trend. First, the surfaces have an increase in the nonpolar character with the increase in nonpolar groups in the pendent chains. Also, the longer hydrocarbon chains are more able to shield the polar ester and amide groups in the backbone. The contact angle measurements of poly(DTBzl carbonate) do not fit in this trend as it contains an aromatic group as the pendent chain. γ_c, γ^d, and γ^p of these polymers are given in Table III. These parameters also decreased with an increase in the chain length of the pendent alkyl groups which is consistent with the low polarity of the hydrocarbon chains. An increase in the length of the pendent chain introduces more hydrocarbon moiety on the surface thus reducing the polarity and surface energy.

Electron Spectroscopy for Chemical Analysis

Surface elemental composition as obtained from the wide scan ESCA spectra of the polycarbonates is listed in Table IV. These values were in close agreement with those expected from the stoichiometry of the repeat unit (Fig. 1). The only elements detected by ESCA were carbon, oxygen, and nitrogen. No indications of surface contaminants were observed within the detection limits of ESCA.

C1s, O1s, and N1s spectra of poly(DTE carbonate) are shown in Figure 2. The C1s, O1s, and N1s spectra for the other polymers were qualitatively similar to those shown in Figure 2. The signal of the CH$_x$ peak increased as the length of the pendent chain increased. Six Gaussian peaks were used in the resolution of the C1s spectra. One

Table II   Contact Angles of Tyrosine-derived Polycarbonates[a]

	Liquids Used				
Polymer	Water (°)	Glycerol (°)	Formamide (°)	Thiodiglycol (°)	Methylene Iodide (°)
Poly(DTE carbonate)	73 (1)	62 (2)	55 (2)	34 (1)	24 (1)
Poly(DTB carbonate)	78 (1)	68 (1)	61 (1)	42 (1)	32 (1)
Poly(DTH carbonate)	87 (1)	72 (1)	67 (1)	54 (1)	41 (2)
Poly(DTO carbonate)	89 (1)	77 (1)	72 (1)	59 (1)	44 (1)
Poly(DTBzl carbonate)	76 (1)	61 (1)	55 (2)	36 (1)	20 (1)

[a] Each value is the average of 18 repetitive measurements for each polymer/liquid combination; standard deviations are shown in parentheses.

Table III Critical Surface Tension (γ_c), Dispersive (γ^d), and Polar (γ^p) Components of the Surface Free Energy of Tyrosine-derived Polycarbonates

Polymer	Surface Free-energy Component		
	γ_c	γ^d	γ^p
Poly(DTE carbonate)	46.4	42.5	3.5
Poly(DTB carbonate)	43.7	40.1	2.4
Poly(DTH carbonate)	40.6	37.5	1.1
Poly(DTO carbonate)	38.5	36.1	0.6
Poly(DTBzl carbonate)	47.6	51.2	0.2

peak was used for CH_x, one for C—O and C—N, one for N—C=O, one for O—C=O, one for the carbonate [O—C(=O)—O], and one for the shake-up satellite ($\pi \rightarrow \pi^*$ transition). O1s spectra were resolved using three peaks corresponding to $\underline{O}$=C—N, $\underline{O}$=C—O, and $\underline{O}$—C=O. The N1s spectra showed the presence of only one nitrogen species. Peak positions were determined by referencing the CH_x peak to 285.0 eV.[25] This peak is the most prominent feature in these spectra and arises from hydrocarbon moieties in the backbone and pendent groups. A small part of this peak could also be due to adventitious hydrocarbon contaminants. However, the elemental composition obtained from wide scans suggests that this contribution is not high (see below).

The resolution of the C1s spectra of tyrosine-derived polycarbonates into component peaks using a least-squares routine was not straightforward. During the fitting process, the solutions of the nonlinear regression algorithm converged to widely different values, which depended critically on the initial estimates of the position and widths of the peaks. This indicated that the solutions of

the fitting routine converged to local minima rather than to the true least-squares solution of the fitting process. Global optimization algorithms[27] may prove useful to obtain the best fit of these types of data. It has been pointed out that there is no way to make sure that the regression has converged to the absolute least-squares solution.[28,29] However, the solution that is selected should have a physical meaning.

To obtain consistent results in the curve resolution process, a constrained fitting of the C1s spectra was used to allow for better initial estimates of peak positions and widths. It has been shown that constraining the solutions can remove the ill-conditioning of the problem; this can be a great advantage when the constraints have a physical basis.[28,29] Thus, the relative areas of the different Gaussian peaks were constrained to the stoichiometric values of the different chemical groups with respect to the carbonate peak; the shake-up peak was left unconstrained. Peak positions and widths were also left unconstrained. When the constrained fitting reached a solution, the constraints were eliminated and the iterative process was run again until a solution was found. The SSI peak fitting software considered that a solution was found when the Chi-square value between two consecutive iterations did not change by more than 0.005. In all cases, a solution was identified based on the above criteria before the program reached 50 iterations, the maximum number of iterations set by us as the calculation cutoff.

By using the forced fitting of the C1s spectra as the initial estimates for the nonlinear least-squares routine, it was possible not only to obtain solutions that were consistent with the stoichiometry of these polymers, but the position and width of the peaks corresponding to the different chemical species were consistent with the values ob-

Table IV Surface Elemental Composition of Tyrosine-derived Polycarbonates

Polymer	% C		% O		% N	
	Measured[a]	Calculated[b]	Measured[a]	Calculated[b]	Measured[a]	Calculated[b]
Poly(DTE carbonate)	75.4	75.0	20.9	21.4	3.7	3.6
Poly(DTB carbonate)	77.2	76.7	19.5	20.0	3.3	3.3
Poly(DTH carbonate)	78.2	78.1	18.5	18.8	3.3	3.1
Poly(DTO carbonate)	79.8	79.4	16.9	17.6	3.3	3.0
Poly(DTBzl carbonate)	79.1	78.8	17.4	18.2	3.5	3.0

[a] Obtained from wide-scan ESCA spectra (0–1000 eV).
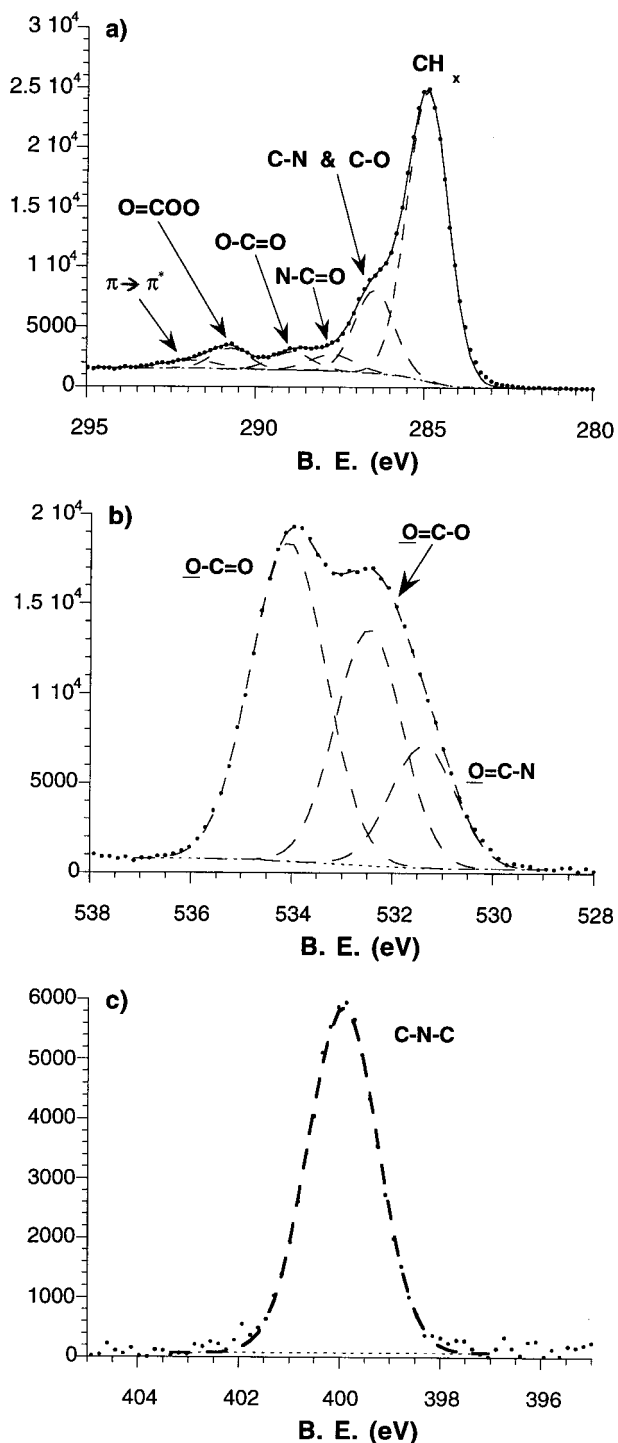[b] Calculated values based on the stoichiometric composition of the polymer repeat unit.

Figure 2 High-resolution ESCA spectra of poly(DTE carbonate): (a) C1s; (b) O1s; (c) N1s.

tained for similar species on other polymeric systems.[25] Because resolution of the C1s spectra of these polymers involved forced fittings for the initial estimates, conclusions derived from the curve fitting of the C1s spectra require corroborating evidence.

Table V lists the peak positions and widths obtained from the curve resolution of the C1s, O1s, and N1s spectra using the procedure described above. Surface compositions obtained from the curve fitting to the high-resolution spectra (C1s, O1s, and N1s) are summarized in Table VI. The close agreement between the surface composition as obtained from ESCA (Tables IV and VI) and the stoichiometry of the repeat unit (Fig. 1) confirms the lack of contamination on these surfaces. As mentioned above, cleanliness of these surfaces cannot be conclusively derived from the resolution of the C1s spectra alone. However, the elemental composition obtained by the wide scan (Table IV), the resolution of the O1s and N1s spectra, and the fact that the positions and widths of the chemical species corresponded to the expected values provided additional corroboration for the absence of significant surface contamination. In particular, if the presence of adventitious hydrocarbon contamination on these surfaces was significant, the wide scan (elemental composition) would have shown a % C appreciably larger than the stoichiometric values. Also, our results indicate that there was no preferential surface orientation of specific moieties of the polymer chain.

The polymer with the benzyl pendent group appears to vary by a large percentage from the expected composition in the resolution of the *C1s spectra* while the elemental composition (Table IV) and the resolution of the *O1s and N1s spectra* (Tables V and VI) are in close agreement to the stoichiometric values. As mentioned before, the resolution of the C1s spectra of these polymers presented numerical difficulties. This was especially true for the polycarbonate with the benzyl pendent group. Thus, the observed variation from the expected composition based on the resolution of the C1s spectra is only of significance if corroborated by other data. However, TOF–SIMS analysis of this polymer (which is extremely sensitive to surface contamination) did not provide evidence for surface contamination (see below).

The assumption that the solution obtained using the constrained fitting as the initial estimates was reasonably close to the true least-squares solution was validated by several factors. First, the surface elemental composition of these polymers was close to the calculated, stoichiometric values. The peak positions corresponded closely to those expected based on the chemical groups present at the surface. Also, the peak positions and widths

Table V   Peak Positions and Widths[a] from the Deconvolution of C1s, O1s, and N1s Spectra for Tyrosine-derived Polycarbonates

| | C1s | | | | | |
| | CH$_x$ (eV) | C—N + C—O (eV) | O=C—O (eV) | O—C=O (eV) | O=COO (eV) | $\pi \to \pi^*$ (eV) |
Pendent Group						
Ethyl	285 (1.4)	286.5 (1.5)	287.2 (1.4)	288.8 (1.6)	290.8 (1.3)	292.0 (2.0)
Butyl	285 (1.5)	286.5 (1.4)	287.5 (1.6)	288.9 (1.5)	290.9 (1.3)	292.2 (2.2)
Hexyl	285 (1.4)	286.5 (1.6)	286.9 (1.2)	288.9 (1.6)	291.0 (1.2)	292.2 (2.2)
Octyl	285 (1.3)	286.5 (1.6)	286.9 (1.8)	288.9 (1.4)	290.9 (1.2)	291.8 (1.9)
Benzyl	285 (1.5)	286.7 (1.2)	288.0 (1.2)	289.1 (1.1)	290.9 (1.1)	291.7 (2.2)

| | O1s | | | N1s |
	O=C—N (eV)	O=C—O (eV)	O=C—O (eV)	C—N—C (eV)
Ethyl	531.4 (1.6)	532.6 (1.6)	534.2 (1.7)	399.9 (1.6)
Butyl	531.4 (1.6)	532.5 (1.6)	534.1 (1.8)	399.9 (1.6)
Hexyl	531.4 (1.5)	532.6 (1.6)	534.2 (1.8)	399.9 (1.6)
Octyl	531.4 (1.7)	532.5 (1.6)	534.1 (1.8)	399.9 (1.6)
Benzyl	531.5 (1.5)	532.6 (1.5)	534.2 (1.8)	400.1 (1.6)

[a] Units are eV; values in parentheses indicate full widths at half-maximum.

Table VI   Surface Composition of Tyrosine-derived Polycarbonates as Obtained from the Deconvolution of C1s, O1s, and N1s Spectra[a]

| | C1s | | | | | |
| | CH$_x$ (%) | C—N + C—O (%) | O=C—O (%) | O—C=O (%) | O=COO (%) | $\pi \to \pi^*$ |
Pendent Group						
Ethyl	68.0 (66.7)	18.4 (19.0)	4.1 (4.8)	5.0 (4.8)	4.5 (4.8)	2.5
Butyl	71.7 (69.6)	16.4 (17.4)	3.3 (4.3)	4.4 (4.3)	4.2 (4.3)	2.3
Hexyl	72.9 (72.0)	16.3 (16.0)	2.6 (4.0)	4.5 (4.0)	3.7 (4.0)	1.8
Octyl	74.1 (74.1)	15.3 (14.8)	3.8 (3.7)	3.4 (3.7)	3.4 (3.7)	1.4
Benzyl	80.4 (73.1)	12.7 (15.4)	2.2 (3.8)	1.9 (3.8)	2.8 (3.8)	4.4

| | O1s | | | N1s |
	O=C—N (%)	O=C—O (%)	O=C—O (%)	C—N—C (%)
Ethyl	16.8 (16.7)	33.4 (33.3)	49.8 (50.0)	100 (100)
Butyl	16.9 (16.7)	32.5 (33.3)	50.6 (50.0)	100 (100)
Hexyl	16.7 (16.7)	33.6 (33.3)	49.7 (50.0)	100 (100)
Octyl	17.0 (16.7)	33.1 (33.3)	49.9 (50.0)	100 (100)
Benzyl	16.9 (16.7)	32.3 (33.3)	50.8 (50.0)	100 (100)

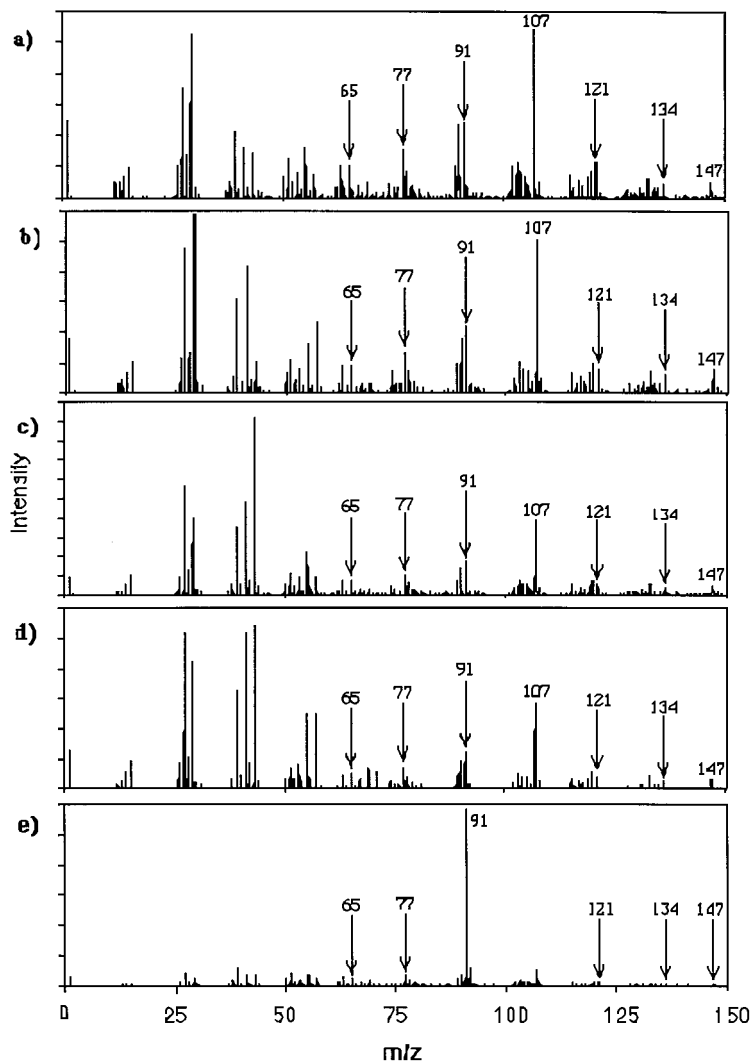[a] Values in parentheses were calculated from structural formulas.

Figure 3 Static SIMS spectra of tyrosine-derived polycarbonates. Positive ions at $m/z = 0-150$. (a) Poly(DTE carbonate); (b) poly(DTB carbonate); (c) poly(DTH carbonate); (d) poly(DTO carbonate); (e) poly(DTBzl carbonate).

were similar among all five polycarbonates, as expected, considering the similarity in the chemical structure between the tested polymers. Additionally, bulk analytical techniques (FTIR and NMR) indicate that these polymers do not have chemical groups other than what is expected from their structural repeat unit (Fig. 1).[14]

Secondary Ion Mass Spectrometry

The positive static SIMS spectra of tyrosine-derived polycarbonates are shown in Figure 3 for $m/z = 0-150$ Daltons. At low masses, the positive SIMS spectra consisted mainly of hydrocarbon peaks ($C_nH_m^+$). For some of these peaks, oxygen-

containing ions also contributed to the signal. For example, at $m/z = 43$, the peak consisted of $C_3H_7^+$ and $C_2H_3O^+$ species, although the contribution of the $C_2H_3O^+$ ion accounted for less than 5% of the signal. Because of the high resolution of the TOF–SIMS instrument employed ($m/\Delta m$ ca. 7000), it was possible to assign unambiguously different species having the same nominal mass ($C_3H_7^+$ and $C_2H_3O^+$ species appear at $m/z = 43$ but their exact masses are 43.0548 and 43.0184, respectively). Peaks that indicate the presence of phenyl rings in the polymer structure were present in spectra for all polymers ($m/z = 65, 77, 91, 105, 115, 152,$ and 178).[30,31] The positive ion SIMS spectra of poly(DTBzl carbonate) showed a peak

at $m/z = 91$ as the dominant feature in this spectrum. This peak corresponds to the tropylium ion (a cyclic $C_7H_7^+$ ion)[31] and is present in the SIMS spectra of each of the five polymers. However, it is more intense for the polymer with a benzyl pendent group. This can be rationalized by the fact that the formation of the tropylium ion from the pendent benzyl group requires breaking one bond, whereas its formation from phenyl rings in the backbone of the polymeric chain requires breaking two bonds. Formation of this ion also requires migration of one H atom when it forms from a benzyl pendent group. Its formation from backbone phenyl rings is a more complex process, requiring migration of more than one H atom and several rearrangements, in addition to the requirement of two broken bonds. This would make the probability of formation of this ion higher from a pendent benzyl group than from a backbone phenyl ring.

At higher masses ($m/z > 100$), the positive ion SIMS spectra showed several peaks originating from fragmentation of the backbone chain of the polymers (Fig. 3). These fragments form via scissions adjacent to ester and amide linkages in the polymers. The structure of these ions are listed in Table VII. Peaks that would allow a facile identification of the pendent groups were not detected in the positive ions SIMS spectra. However, the positive SIMS spectrum of each of these polymers showed a characteristic fragmentation pattern that provided a spectral fingerprint (Fig. 3).

The negative ion SIMS spectra of the tyrosine-derived polycarbonates are given in Figures 4 and 5 for $m/z = 40–130$ and $m/z = 120–280$, respectively. The most intense peaks in the negative ion SIMS spectra of these polymers are peaks corresponding to H^-, C^-, CH^-, O^-, OH^-, and CN^- species. Other peaks also present in spectra of each of the polymers were $m/z = 42$ and 58, which correspond to the following structures:

$$O=C=N^- \qquad {}^-H_2C-\overset{\overset{\textstyle O}{\|}}{C}-NH_2$$

$$m/z = 42 \qquad\qquad m/z = 58$$
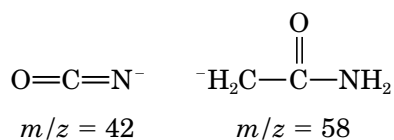
In the low mass range ($m/z = 40–130$), peaks characteristic of the pendent chains were observed at masses of 43 and 45 for the ethyl pendent groups ($C_2H_3O^-$ and $C_2H_5O^-$), 71 and 73 for the butyl pendent groups ($C_4H_7O^-$ and $C_4H_9O^-$), 99 and 101 for the hexyl pendent groups ($C_6H_{11}O^-$ and $C_6H_{13}O^-$), and 127 for the octyl pendent

Table VII   Ion Structure Assignments of Tyrosine-derived Polycarbonates for the Positive SIMS Spectra in Higher Mass Range ($m/z > 100$)

Ion Structure	Mass/Charge
	107
$HO-\langle\bigcirc\rangle-C\equiv C+$	117
$HO-\langle\bigcirc\rangle-\overset{+}{C}=CH_2$	119
$HO-\langle\bigcirc\rangle-\overset{+}{C}H-CH_3$	121
$HO-\langle\bigcirc\rangle-CH=C=\overset{+}{N}H_2$	134
$HO-\langle\bigcirc\rangle-CH=CH-C\equiv\overset{+}{O}$	147
$HO-\langle\bigcirc\rangle-CH_2-CH_2-C\equiv O+$	149
$HO-\langle\bigcirc\rangle-CH_2-CH_2-\overset{\overset{\textstyle +}{\overset{\textstyle OH}{\|}}}{C}-\overset{\bullet}{N}H$	165
$HO-\langle\bigcirc\rangle-CH_2-CH-\overset{\bullet+}{N}H_2$ with $-C=O$ and $-OH$	181

group ($C_8H_{15}O^-$). These peaks are labeled in Figure 4 to facilitate their identification. For poly(DTBzl carbonate), the peak characteristic of the benzyl pendent group would appear at $m/z = 107$ but, at this mass, an ion also originates from fragmentations of the backbone of the polymers.

At higher masses, peaks originating from fragmentation of the polymeric backbone appear in the negative ion SIMS spectra of the five polymers. Ion structure assignments for these peaks are given in Table VIII. The peak with $m/z = 107$ could also be formed from fragmentation of a pendent benzyl group. This may explain the increased intensity of this peak in the negative ion SIMS spectra of poly(DTBzl carbonate) over the rest of the polymers. In the high mass range,
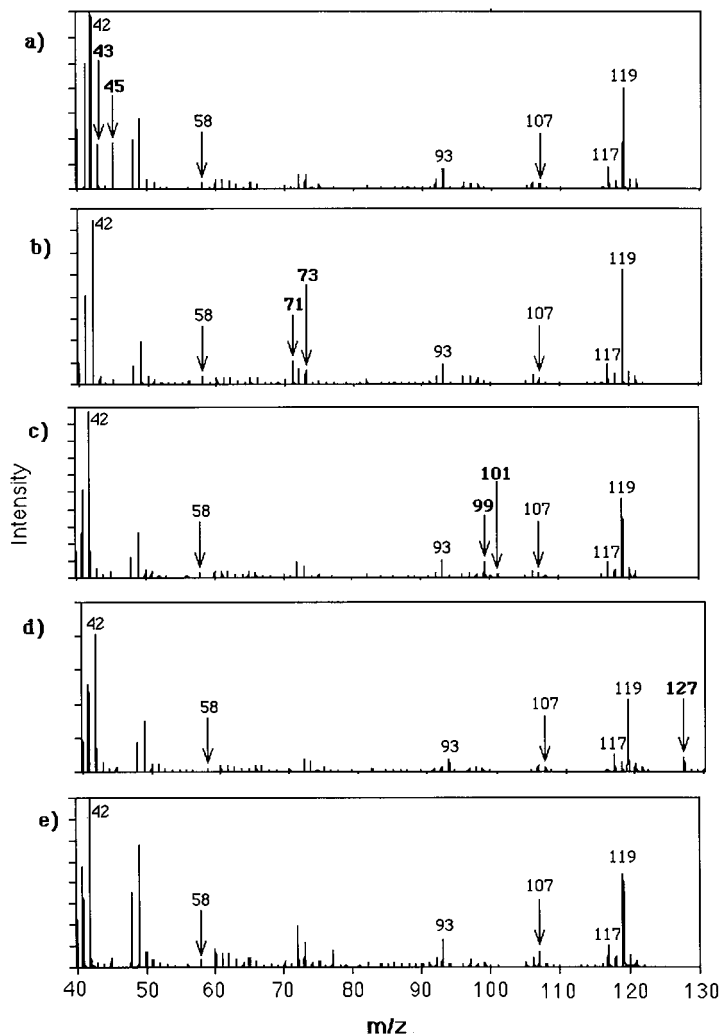
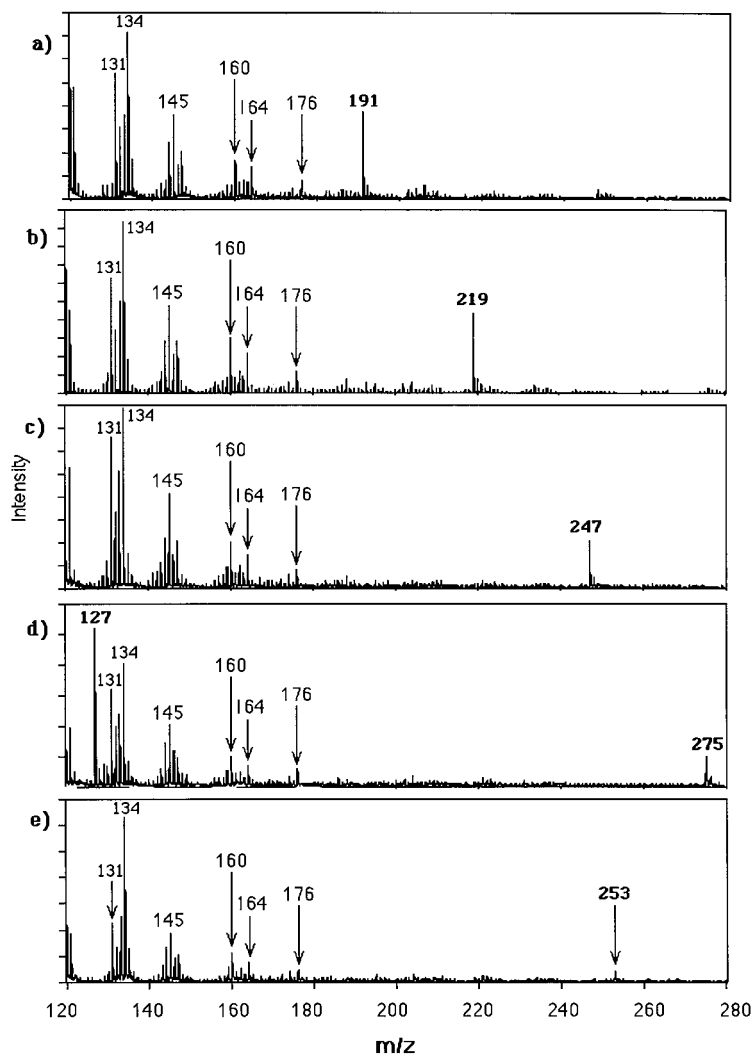**Figure 4**   Static SIMS spectra of tyrosine-derived polycarbonates. Negative ions at $m/z = 40$–130. (a) Poly(DTE carbonate); (b) poly(DTB carbonate); (c) poly(DTH carbonate); (d) poly(DTO carbonate); (e) poly(DTBzl carbonate). Peaks indicative of pendent groups are labeled in boldface.

a series of peaks whose structure resembled a fragment of the polymeric backbone with the pendent groups attached were identified. These peaks appeared at m/z of 191, 219, 247, and 275 for the polycarbonates with an ethyl, butyl, hexyl, and octyl groups, respectively. These peaks are separated by 28 mass units, consistent with the difference in length of the pendent alkyl chains, $(CH_2-CH_2)_n$ with $n = 1, 2$, and 3 with respect to poly(DTE carbonate). For poly(DTBzl carbonate), the peak related to the fragment of the backbone with the benzyl pendent chain attached appeared at $m/z = 253$. The structure of these ions are given in Table IX. These peaks provide a straightforward way to identify each of the five

tyrosine-derived polycarbonates based on their negative SIMS spectra. It should also provide a reference peak to study the hydrolysis of the pendent groups during surface degradation or deprotection of the pendent groups to attach bioactive molecules.

The fact that TOF–SIMS was dominated by fragments that were expected based on the chemistry of these polymers suggests that surface contamination was much less than a monolayer (the sampling depth of SIMS for polymers is about 10–15 Å). If large parts of the polycarbonate surfaces were covered by adventitious hydrocarbon contaminants, peak signals arising from these surfaces would not have been so prominent. Rather,

Figure 5 Static SIMS spectra of tyrosine-derived polycarbonates. Negative ions at m/z = 120–280. (a) Poly(DTE carbonate); (b) poly(DTB carbonate); (c) poly(DTH carbonate); (d) poly(DTO carbonate); (e) poly(DTBzl carbonate). Peaks indicative of pendent groups are labeled in boldface.

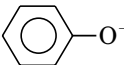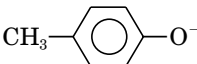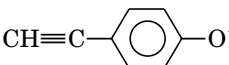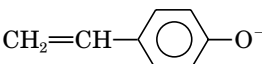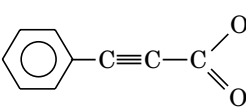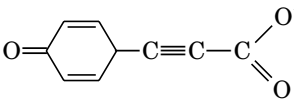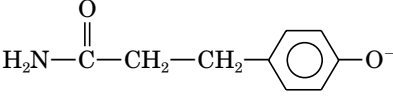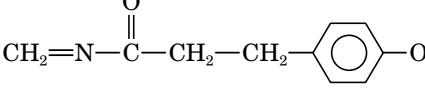the spectra would have been dominated by $C_nH_m^+$ species.

CONCLUSIONS
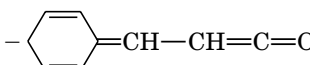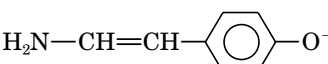
The surface characterization of the tyrosine-derived polycarbonates described here complements previous studies about the biocompatibility of these polymers. Because of the low level of contamination of the materials studied, they can serve as reference standards for future surface characterization studies of these and analogous polymers, such as the tyrosine-derived polyiminocarbonates and polyarylates.

Contact angle measurements of the homologous series of four of the tyrosine-derived polycarbonates found the wettability to decrease with the increasing length of the pendent chain. A decrease in surface energy and polarity of these polymers with increasing chain length was consistent with the increased amount of hydrocarbon moieties at the surface for longer hydrocarbon chains.

The curve resolution of the C1s ESCA spectra of these polymers did not yield physically meaningful results without first introducing constraints in the least-squares fitting routine. By using the constrained fitting as the initial estimates in the least-squares fitting routine, it was possible to remove the ill-conditioning of the prob-

lem and also to obtain results that were physically meaningful. The numbers obtained were consistent with the chemical structure, peak positions, and widths of the peaks corresponding to the different chemical groups in the spectra. The fact that the stoichiometry of these polymers (elemental composition) and the deconvolution of the O1s and N1s spectra agreed with the stoichiometry of the repeat unit supports the hypothesis that the

Table VIII Ion Structure Assignments of Tyrosine-derived Polycarbonates for the Negative SIMS Spectra in Higher Mass Range ($m/z > 100$)

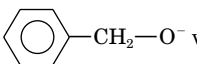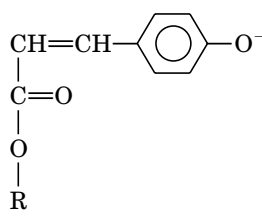| Ion Structure	Mass/Charge
⟨benzene⟩—O⁻	93
CH₃—⟨benzene⟩—O⁻	107[a]
CH≡C—⟨benzene⟩—O⁻	117
CH₂=CH—⟨benzene⟩—O⁻	119
⁻⟨ring⟩=CH—CH=C=O	131
H₂N—CH=CH—⟨benzene⟩—O⁻	134
⟨benzene⟩—C≡C—C(O⁻)(=O)	145
O=⟨ring⟩—C≡C—C(O⁻)(=O)	160
H₂N—C(=O)—CH₂—CH₂—⟨benzene⟩—O⁻	164
CH₂=N—C(=O)—CH₂—CH₂—⟨benzene⟩—O⁻	176

[a] At $m/z = 107-$, the fragment ion ⟨benzene⟩—CH₂—O⁻ was generated by direct scission of a pendent benzyl group in poly(DTBzl carbonate).

Table IX Ion Structure Assignment for Peaks Characteristic of Pendent Groups of Tyrosine-derived Polycarbonates

CH=CH—⟨benzene⟩—O⁻
|
C=O
|
O
|
R

Pendent Chain (R)	Mass/Charge
Ethyl	191
Butyl	219
Hexyl	247
Octyl	275
Benzyl	253

fitting was close to the true least-squares solution. In addition, there was consistency in peak positions and widths for the different chemical groups among the five polymers studied. The close agreement between surface composition as obtained by ESCA and the theoretical values obtained from the repeat unit of these polymers demonstrated the cleanliness of these surfaces.

The positive ion SIMS spectra of these polymers showed ion structures characteristic from the fragmentation of the polymeric backbone. At low masses, the positive SIMS spectra consisted mainly of $C_nH_m^+$ peaks with a small contribution from oxygen-containing ions. Peaks characteristic of the pendent groups could not be distinguished in the positive ion SIMS spectra. However, the fragmentation pattern provided a fingerprint spectrum for each polymer.

The negative ion SIMS spectra showed peaks corresponding to ion structures originating from fragmentation of the polymeric backbone and also from the pendent groups. At high masses, a series of peaks containing information about the backbone and the pendent groups could be used to distinguish each of the polymers. These peaks can provide a point of reference to study surface degradation of these polymers or to monitor hydrolytic deprotection of the pendent groups.

It is the exception to find polymers where the surface structure closely resembles the bulk structure.[32] More commonly, surface contamination,[33] surface-active additives,[34] surface reaction (e.g., oxidation), or surface localization of specific chain segments[35] lead to a surface composition appreci-

ably different from that measured in the bulk. The cleanliness and absence of surface segregation in these tyrosine-derived polycarbonates suggests applications as reference standards and as models for systematically relating surface composition to biological reaction.[36] The freedom from surface contamination also portents well for the application of these materials *in vivo* where surface films can trigger undesirable cellular and tissue responses.[37]

REFERENCES

1. R. B. Bourne, H. Bitar, P. R. Andreae, L. M. Martin, J. B. Finlay, and F. Marquis, *Can. J. Surg.,* **31**(1), 43 (1988).
2. O. M. Böstman, *J. Bone J. Surg.,* **73**(1), 148 (1991).
3. R. Langer, *Science,* **Sept. 28,** 1527 (1990).
4. J. P. Vacanti, M. A. Morse, W. M. Saltzman, A. J. Domb, A. Perez-Atayade, and R. Langer, *J. Pediatr. Surg.,* **23,** 3 (1988).
5. C. A. Vacanti, R. Langer, B. Schloo, and J. P. Vacanti, *Plast. Reconstr. Surg.,* **88**(5), 753 (1991).
6. B. D. Ratner, A. B. Johnston, and T. J. Lenk, *J. Biomed. Mater. Res. Appl. Biomat.,* **21**(A1), 59 (1987).
7. B. D. Ratner, D. G. Castner, T. A. Horbett, T. J. Lenk, K. B. Lewis, and R. J. Rapoza, *Vac. Sci. Technol. A,* **8**(3, Part 2), 2306 (1990).
8. J. Kohn and R. Langer, *J. Am. Chem. Soc.,* **109,** 817 (1987).
9. J. Kohn, *Trends Polym. Sci.,* **1**(7), 206 (1993).
10. J. Kohn, in *Biodegradable Polymers as Drug Delivery Systems,* M. Chasin and R. Langer, Eds., Marcel Dekker, New York, 1990, p. 195.
11. C. H. Bamford, A. Elliot, and W. E. Hanby, in *Physical Chemistry—A Series of Monographs,* E. Hutchinson, Series Ed., Academic Press, New York, 1956, Vol. 5.
12. S. Pulapura, C. Li, and J. Kohn, *Biomaterials,* **11,** 666 (1990).
13. S. Pulapura and J. Kohn, *Biopolymers,* **32,** 411 (1992).
14. S. I. Ertel and J. Kohn, *J. Biomed. Mater. Res.,* **28,** 919 (1994).
15. J. Fiordeliso, S. Bron, and J. Kohn, *J. Biomater. Sci. (Polym. Ed.),* **5**(6), 497 (1994).
16. F. H. Silver, M. Marks, Y. P. Kato, C. Li, S. Pulapura, and J. Kohn, *J. Long-Term Effects Med. Implants,* **1**(4), 329 (1992).
17. S. I. Ertel, J. Kohn, M. C. Zimmerman, and J. R. Parsons, *J. Biomed. Mater. Res.,* **29**(11), 1337 (1995).
18. J. Choueka, J. L. Charvet, K. J. Koval, H. Alexander, K. S. James, K. A. Hooper, and J. Kohn, *J. Biomed. Mater. Res.,* **31,** 35 (1996).
19. K. A. Hooper and J. Kohn, *J. Bioact. Compat. Polym.,* **10**(4), 327 (1995).
20. Y. C. Ko, B. D. Ratner, and A. S. Hoffman, *J. Coll. Interf. Sci.,* **82,** 25 (1981).
21. W. A. Zisman, in *Contact Angle, Wettability and Adhesion,* F. M. Fowkes, Ed., ACS Advances in Chemistry Series, Vol. 43, American Chemical Society, Washington, DC, 1964, p. 1.
22. D. H. Kaelble, *J. Adhes.,* **2,** 66 (1970).
23. D. H. Kaelble and K. C. Uy, *J. Adhes.,* **2,** 50 (1970).
24. J. H. Scofield, *J. Electron Spectrosc. Relat. Phenom.,* **8**(2), 129 (1976).
25. A. Dilks, in *Electron Spectroscopy: Theory, Techniques, and Applications,* A. D. Baker and C. R. Crundle, Eds., Academic Press, London, 1981, Vol. 4, p. 277.
26. D. Briggs and M. J. Hearn, *Vacuum,* **36**(11–12), 1005 (1986).
27. T. Aimo and A. Zhilinskas, *Global Optimization,* Springer-Verlag, New York, 1989.
28. G. Leclerc and J. J. Pireaux, *J. Electron Spectrosc. Relat. Phenom.,* **71**(2), 141 (1995).
29. G. Leclerc and J. J. Pireaux, *J. Electron Spectrosc. Relat. Phenom.,* **71**(2), 179 (1995).
30. D. Briggs, A. Brown, and J. C. Vickerman, *Handbook of Static Secondary Ion Mass Spectrometry (SIMS),* Wiley, Chichester, 1989.
31. W. J. Van Ooij and H. G. Brinkhuis, *Surf. Interf. Anal.,* **11**(8), 430 (1988).
32. B. D. Ratner and D. G. Castner, *Coll. Surf. B. Biointerf.,* **2,** 333 (1994).
33. B. D. Ratner, in *Treatise on Clean Surface Technology,* K. L. Mittal, Ed., Plenum Press, New York, 1987, Vol. I, p. 247.
34. B. D. Ratner, in *Physicochemical Aspects of Polymer Surfaces,* K. L. Mittal, Ed., Plenum, New York, 1983, Vol. 2, p. 969.
35. S. C. Yoon, B. D. Ratner, B. Ivan, and J. P. Kennedy, *Macromolecules,* **27,** 1548 (1994).
36. B. D. Ratner and A. S. Hoffman, in *Synthetic Biomedical Polymers. Concepts and Applications,* M. Szycher and W. J. Robinson, Eds., Technomic, Westport, CT, 1980, Vol. 1, p. 133.
37. B. D. Ratner, *Arch. Ophthalmol.,* **101,** 1434 (1983).